

Article

Analyzing the Characteristics of UHI (Urban Heat Island) in Summer Daytime Based on Observations on 50 Sites in 11 LCZ (Local Climate Zone) Types in Xi'an, China

Yunwei Zhang^{1,2,*}, Jili Zhang¹, Xiaoqian Zhang¹, Dian Zhou¹ and Zhaolin Gu^{1,*}

¹ School of Human Settlements and Civil Engineering, Xi'an Jiaotong University, Xi'an 710049, China; zhangjili@stu.xjtu.edu.cn (J.Z.); zqx0313@stu.xjtu.edu.cn (X.Z.); dian-z@mail.xjtu.edu.cn (D.Z.)

² State Key Laboratory of Loess and Quaternary Geology, Institute of Earth Environment, CAS, Xi'an 710061, China

* Correspondence: zhangyunwei@mail.xjtu.edu.cn (Y.Z.); guzhaolin@mail.xjtu.edu.cn (Z.G.)

Abstract: Urbanization has induced significant changes on local climate in urban areas. For sustainable urban planning, it is necessary to identify the distribution characteristics of urban heat island (UHI) and the effects of land cover properties. In situ measurements are frequently carried out to obtain critical data in urban climate studies. However, long-time continuous observations on multiple sites are still rare, even though they would be useful in mapping the distribution of UHI intensity. In the current work, three observation campaigns were carried out in Xi'an, China. Pedestrian-level air temperatures (PLAT) were measured with portable micro-environment stations on 50 sites in 11 local climate zone (LCZ) types. The normalized PLAT was used to investigate the canopy layer UHI characteristics and the effects of LCZ types. Results revealed that the land coverage type and the surface structure have significant influence on the local climate. The PLAT in high-surface-fraction building covered areas was higher than that in low-surface-fraction building covered areas. In areas with similar building surface fraction, building height influences the UHI magnitude as well, as tall buildings would provide more shielding on the pedestrian level. The average UHI magnitude and the standard deviation within each LCZ type were calculated by statistical analysis of the observed results, which proved to be useful for UHI mapping based on the LCZ classification results in urban areas.

Keywords: urban heat island (UHI); local climate zone; land use; in situ measurement; normalized temperature; urban climate map



Citation: Zhang, Y.; Zhang, J.; Zhang, X.; Zhou, D.; Gu, Z. Analyzing the Characteristics of UHI (Urban Heat Island) in Summer Daytime Based on Observations on 50 Sites in 11 LCZ (Local Climate Zone) Types in Xi'an, China. *Sustainability* **2021**, *13*, 83. <https://doi.org/10.3390/su13010083>

Received: 26 November 2020

Accepted: 21 December 2020

Published: 23 December 2020

Publisher's Note: MDPI stays neutral with regard to jurisdictional claims in published maps and institutional affiliations.



Copyright: © 2020 by the authors. Licensee MDPI, Basel, Switzerland. This article is an open access article distributed under the terms and conditions of the Creative Commons Attribution (CC BY) license (<https://creativecommons.org/licenses/by/4.0/>).

1. Introduction

With rapid urbanization, more and more people migrate to urban areas. The urbanization ratio in China has increased from 17.92% in 1978 to 58.52% in 2017 [1]. The underlying surface structure in urban areas have been changed dramatically by decreasing of vegetation ratio and increasing of impervious surface, which result in serious environmental issues, e.g., the urban heat island (UHI) problems [2–4].

The UHI intensity could be denoted as air temperature differences between urban and rural area [5]. Thus, the selection of temperature measurement sites is important. It has been verified that the calculated UHI intensities with measured air temperatures on different sites would be different. Based on summarizing previous studies, Stewart and Oke [6] proposed the method of local climate zone (LCZ) by distinguishing the structure of urban canopy layer. The LCZ scheme with a total of 17 LCZ types, including ten “built types” (LCZ 1–LCZ 10) and seven “land cover types” (LCZ A–LCZ G). The 17 LCZ types are compact high-rise (LCZ 1), compact mid-rise (LCZ 2), compact low-rise (LCZ 3), open high-rise (LCZ 4), open mid-rise (LCZ 5), open low-rise (LCZ 6), lightweight low-rise (LCZ 7), large low-rise (LCZ 8), sparsely low-rise (LCZ 9), heavy industry (LCZ 10), densely covered with

trees (LCZ A), patchy covering of scattered trees (LCZ B), existence of bushes/scrub (LCZ C), low plants (LCZ D), bare rock/covered with paving tiles (LCZ E), covered with bare soil (LCZ F) and existence of water body (LCZ G). The LCZ method has been verified to be clear standard and wide adaptable in urban climate mapping [7–11]. The classification methods of LCZ have been widely investigated as well [12–14]. The world urban database and access portal tools (WUDAPT) method proposed by Bechtel et al. [12] has been frequently used, which is illustrated by high accuracy in LCZ classifications [15]. An idealized LCZ classification process could be divided into three steps by WUDAPT method: pre-process using the Landsat data, training selected samples and LCZ classification [12,13]. With the WUDAPT method used in Xi'an, He et al. [13] divided the building height into four levels, which are low-rise, mid-low-rise, mid-high-rise and high-rise buildings, according to the building height variation characteristics in urban areas of China.

Comparative studies have shown that LCZ classification is suitable to investigate the surface urban heat island (SUHI) [7,11,16,17]. Cai et al. [7] pointed out that the land surface temperatures were generally consistent with LCZ types, with higher land surface temperatures observed in built-up LCZ types. They also proposed some in situ measured air temperatures. Stewart and Oke [6] compared the air temperature difference between LCZ types. They also verified that LCZ scheme can use the inter-zone temperature difference to quantify the urban canopy layer UHI intensity [18,19]. Recently, some studies have evaluated the relation between air temperature and LCZ types [19–24]. It seems that the measurement method of air temperature is a key issue influencing the results of these studies.

The mobile monitoring method was proposed to try to measure air temperatures on multiple sites. As the air temperatures on different sites were usually measured non-simultaneously, thus, a normalization on the measured data was required [25,26]. The mobile monitoring method has been widely used in urban canopy layer heat island investigations [18,22,27,28]. The main advantage of the mobile monitoring method is that air temperatures on multiple sites could be measured with limited equipment. However, in a mobile observation, only a short time (in minutes) measurement was carried out on each site. Liu et al. [22] conducted the mobile observation with an electric bicycle in speed of 20 km/h along a 14 km route, throughout 18 blocks. In the mobile monitoring, a stationary reference station was needed for data normalization [22,28]. Stationary weather stations would get long-time (for days) continuous air temperature data. Beck et al.'s [20] used measured air temperatures on a meteorological network with 80 logger sites, in which quasi continuous observations were available for about 40 sites. They revealed that temperature difference among LCZs are not restricted to "ideal" synoptic clear evidence, but occur also under disturbed conditions. However, meteorological networks with tens of sites are still rare. Measurement coupled with the stationary meteorological stations and portable micro-environment stations (PMS), which is similar to the mobile monitoring method, but in larger horizontal areas, would be more reasonable for studying the urban scale UHI distribution characteristics [29,30].

A lot of investigations focused on qualitative analysis of the influence of surface structure, coverage, material and human activities on different LCZ types. However, in practice, sustainable urban planning requires not only the local thermal conditions in different LCZ types, but also the overall UHI map and/or even the comprehensive urban climate map [29,31–33]. Till now, the canopy UHI mapping model in urban areas, especially empirical model based on measured data, is still rare. The main difficulty is the measurement on air temperatures, as it requires simultaneous multi-site observation over all the LCZ types. Many investigations have discovered the high correlation between the urban canopy layer UHI intensity and the LCZ type [18–24]. However, the main way to map UHI distributions is still the spatial interpolation method [34], which would be unreasonable, as the land cover characteristics of urban canopy layer do not always vary continuously in the horizontal space. Thus, an empirical UHI mapping model based on the LCZ classification results would provide more reasonable UHI distribution characteristics.

In the current work, three observation campaigns were carried out in Xi'an, a mega city of Northwestern China. A quasi-continuous method combining the PMS and the stationary meteorological station was proposed to measure the daytime air temperature at the pedestrian level on 50 sites in 11 LCZ types. The measured pedestrian-level air temperatures (PLAT) were normalized as those usually processed in the mobile monitoring. The normalized air temperatures were used to analyze the influence of LCZ types on canopy layer UHI, then an empirical UHI mapping model was proposed and applied to establish the daytime UHI map in urban areas of Xi'an based on the LCZ classification results.

2. Methods

The urban areas are divided into blocks by the road network. Each block was given a theme in urban planning with designated criteria on building height, afforestation rate, etc. Thus, one block usually presents characteristics of a certain LCZ type [6]. Blocks in the urban area could be classified into different LCZ types [13]. In the current work, typical blocks representing different LCZ types were selected, in which PMSs were set up to measure the PLAT quasi-continuously [20]. The measured data were normalized as those usually processed in mobile observations [22,27–30].

2.1. Site Description

Xi'an is the capital of Shaanxi province in China. It is also a famous historical and cultural city. It locates in the center of the Guanzhong Basin in northwestern China (107.4° – 109.5° East, 33.5° – 34.5° North). Xi'an experiences four distinct seasons with hot summer, annually averaged air temperature, mean relative humidity and mean wind speed of 27.2°C , 70% and 1.6 m/s, respectively, and a northeastern prevailing wind [34]. There are Qinling Mountains in the south and Loess Plateau in the north. The study of the current work was carried out in the main urban areas of Xi'an, mainly inside the third ring road, as shown in Figure 1. The target area was about 150 km^2 .

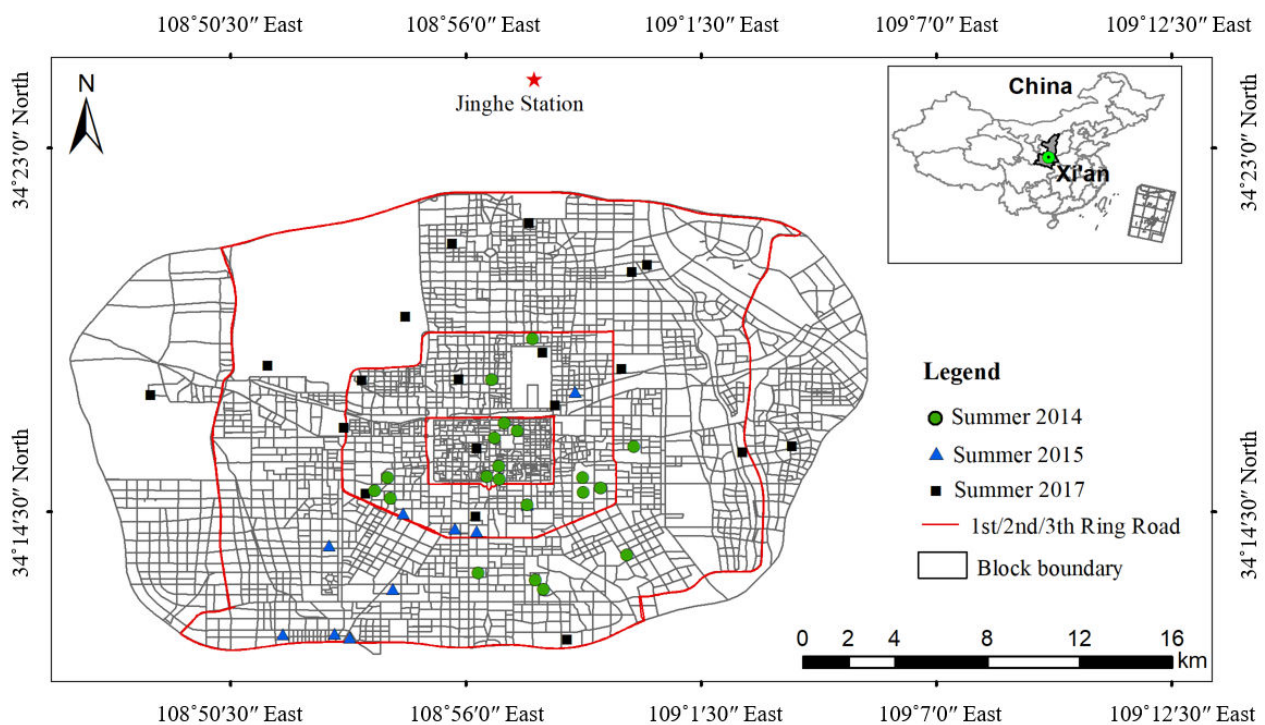


Figure 1. Location of Xi'an and distribution of the measurement sites.

2.2. LCZ Classification and Distribution of Measurement Sites

In the current work, the main urban areas within the third ring road of Xi'an were divided into LCZs. The LCZ classification method proposed by Bechtel et al. [12] and He et al. [13] was used. According to the situation in Chinese cities, buildings could be divided into four categories with different height: low-rise buildings (three stories or below), multi-story buildings (or mid-low-rise buildings, 4–6 stories), mid-high-rise buildings (7–15 stories) and high-rise buildings (16 stories or more). In the current classification system, the building heights of LCZ 5 were subdivided into two types: "LCZ 5-1" with open mid-high-rise buildings, and "LCZ 5-2" with open mid-low-rise buildings. The currently used LCZ classification system is shown in Table 1. The WUDAPT method [12] was used in preparing the LCZ map by three steps: pre-processing the Landsat data, selecting and training samples, and LCZ classification with the software of SAGA-GIS [35].

Table 1. Classification of LCZ (local climate zone) types with modification of definitions given by Stewart and Oke et al. [12,13].

Building Types	Land Cover Types
LCZ 1: Compact high-rise	LCZ A: Densely covered with trees
LCZ 2: Compact mid-rise	LCZ B: Patchy covering of scattered trees
LCZ 3: Compact low-rise	LCZ C: Existence of bushes, scrub
LCZ 4: Open high-rise	LCZ D: Low plants
LCZ 5 (i) Open mid-high-rise (ii) Open mid-low-rise	LCZ E: Bare rock/covered with paving with bare paving tiles
LCZ 6: Open low-rise	LCZ F: Covered with bare soil
LCZ 7: Lightweight low-rise	LCZ G: Existence of water bodies
LCZ 8: Large low-rise	
LCZ 9: Sparsely low-rise	
LCZ 10: Heavy industry	

- (1) Pre-processing the Landsat data: The target area was determined by clipping the Landsat images. This pre-processed image was re-sampled in a resolution of 100 to 150 m, in order to get the spectral signal that representing the local-scale urban structures (e.g., buildings in the block), rather than a single smaller object (e.g., one or part of a building).
- (2) Selecting and training samples: Following the former studies [6,12,13], typical blocks of the representative geometric and/or surface cover properties were selected by polygons as the training samples of each LCZ type, which was then saved as a "/*.kml" data. Training samples of 13 LCZ types were found in the target area.
- (3) LCZ classification using the software "SAGA-GIS": The pre-processed Landsat images and the selected training sampled data (the "/*.kml" data) were imported into the software SAGA-GIS [35]. Using the SAGA-GIS, the LCZ classification in the study area was calculated and conducted with a random forest classifier by comparing the similarity between the training samples and the blocks in the study area.

The main urban area of Xi'an was divided into 2771 blocks by the road network. With the WUDAPT method, these 2771 blocks were classified into 13 LCZ types, which are LCZ 1, LCZ 2, LCZ 3, LCZ 4, LCZ 5 (subdivided into LCZ 5-1 and LCZ 5-2), LCZ 6, LCZ 8, LCZ 10, LCZ B, LCZ D, LCZ E, LCZ F and LCZ G. Only several blocks are LCZ F or LCZ G. Figure 2 shows the LCZ map of the study area. Fifty typical blocks were selected as the measurement sites to observe the PLAT with PMSs. The 50 measurement sites correspond to 11 LCZ types, as shown in Table 2. Figure 1 also showed the horizontal distribution of these 50 measurement sites.

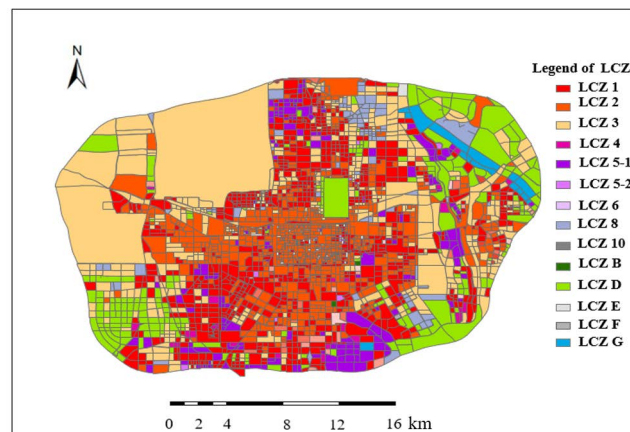


Figure 2. Local climate zone (LCZ) map of the study area.

Table 2. Local climate zone (LCZ) type and the measured and normalized air temperatures on the measurement sites.

Measurement Site Number	LCZ Type	Measured Average Air Temperature (°C)	Normalized Average Air Temperature (°C)
1	LCZ 6	39.3	35.6
2	LCZ D	33.2	33.8
3	LCZ 6	37.5	33.4
4	LCZ 2	32.8	35.9
5	LCZ 3	33.9	32.5
6	LCZ 3	29.2	33.1
7	LCZ 1	34.8	34.5
8	LCZ 2	37.5	38.3
9	LCZ 5-1	30.0	34.6
10	LCZ 5-2	34.6	33.2
11	LCZ 5-2	30.4	33.5
12	LCZ 1	33.9	34.1
13	LCZ 3	36.2	34.1
14	LCZ 3	31.4	35.1
15	LCZ 8	33.5	34.6
16	LCZ 2	36.5	35.9
17	LCZ 2	31.3	35.1
18	LCZ 3	39.3	38.3
19	LCZ 4	29.2	33.5
20	LCZ 8	34.3	35.2
21	LCZ E	31.1	35.6
22	LCZ 8	36.1	34.8
23	LCZ 5-1	33.4	33.2
24	LCZ 8	33.0	38.5
25	LCZ B	32.0	36.5
26	LCZ 8	35.1	35.5
27	LCZ 2	29.2	36.8
28	LCZ E	33.9	35.4
29	LCZ 2	25.0	36.3
30	LCZ D	33.0	32.9
31	LCZ 2	34.9	33.2
32	LCZ 5-1	35.6	32.4
33	LCZ 5-1	30.8	33.1
34	LCZ 2	29.4	29.9
35	LCZ 4	34.0	33.1
36	LCZ 2	33.1	30.6
37	LCZ 5-2	39.7	33.1
38	LCZ 5-1	37.6	34.6
39	LCZ 5-2	34.0	37.1
40	LCZ 2	35.7	32.1
41	LCZ 8	28.1	35.1
42	LCZ 5-1	38.7	32.8
43	LCZ 6	29.9	29.9
44	LCZ 2	36.9	37.3
45	LCZ 2	35.5	32.3
46	LCZ 5-1	33.9	34.1
47	LCZ 5-2	35.0	31.9
48	LCZ 5-1	31.0	35.1
49	LCZ B	35.1	28.8
50	LCZ 6	29.6	34.2

2.3. Measurement Campaign and Equipment

The current work was part of the National Science and Technology Foundation Project of “Comprehensive survey of human settlement quality and preparation of urban climate map for typical cities” (here, we denote it as “CS-UC project”), which was supported by the Ministry of Science and Technology of the People’s Republic of China (see also Luo et al. [36], Xu et al. [29,34] and Zhang et al. [30]). In the CS-UC project, air temperature, relative humidity, wind speed and direction, concentration of PM_{10} and NO_x were observed in seven cities (Xi’an, Wuhan, Dalian, Yulin, Luoyang, Foshan and Taizhou). PMSs were used to measure the daytime PLAT, relative humidity, wind speed and direction. In the current work, the TR-72WF temperature and humidity recorders were used to measure the air temperature [37], which was tied to a tripod at 1.5–1.7 m above the ground, as shown in Figure 3. The TR-72WF was portable, with a size of $55 \times 78 \times 18$ mm, high resolution ratio ($0.1 \text{ }^\circ\text{C}$) and accuracy ($0.5 \text{ }^\circ\text{C}$). There is an air pass channel and a thermistor to measure air temperature, within a wide range from $-10 \text{ }^\circ\text{C}$ to $60 \text{ }^\circ\text{C}$. The storage frequency of the data logger was set to be 1 min. The wind speed and direction was observed by ultrasonic anemometers. The accuracy for wind speed is 0.3 m/s and for wind direction is $0.1 \text{ }^\circ\text{C}$.



Figure 3. View of the portable micro-environment stations (PMS), equipment and the surrounding environment.

Three observation campaigns were executed in the summer of the years 2014, 2015 and 2017, with measurement on 20, 11 and 19 sites, respectively. In the observation campaigns, the PMSs were placed on sites representative of the land cover features, and also where people frequently visit, e.g., roadside, inside the entrance of a community and little squares. Figure 3a shows a case where the PMS was placed on a roadside in a community. The observed data represents the exposed micro-climate conditions of residents. Different from the former mobile measurements, the PMSs in the current work were not moving with cars or motorcycles, but were carried to another site after three days’ observation on one site. For all the 50 typical blocks, the measurements were carried out on different days quasi-continuously [20]. Thus, normalization on the measured air temperature are demanded before doing the comparative analysis.

2.4. Normalization on the Measured Air Temperatures

Mobile measurement was frequently used in UHI investigations [22,26–28,38,39]. Unger et al. [28] showed that the temporal variations of temperature difference were affected by cloudiness, wind speed and land-use conditions. Leconte et al. [40] evaluated the mobile measurement method for UHI assessment on LCZs in a local scale area about 8 km². Liu et al. [22] proposed an integrated method of mobile measurement in local scale areas less than 10 km².

It should be noted that the former studies with mobile measurement were carried out in a local area, thus, the measurements were carried out in a period of several hours and nearby weather stations were selected as stationary reference stations [22,40,41]. In the current work, measurements were carried out in the urban scale in 3 observation campaigns. Thus, a simplified normalization method was used in the current work, by calculating the normalization coefficient with the air temperature measured on PMS over that measured on the stationary reference station. The normalization coefficient could be calculated by Equation (1), and the city's background meteorological station (Jinghe station, as shown in Figure 1) was selected as the stationary reference station.

$$C_i = \frac{\bar{T}_i}{\bar{T}_S}, \quad (1)$$

where, C_i is the normalization coefficient of the i^{th} measurement site, i is the measurement site number, \bar{T}_i and \bar{T}_S are the average air temperatures measured on the PMS and the stationary reference station in the same period of time, respectively. The reference air temperature is denoted as T_R , thus, the normalized average air temperature of the i^{th} PMS (denoted as $T_{N,i}$) could be estimated by Equation (2). The purpose of proposing reference air temperature (T_R) was to provide a reference value for comparison. Thus, average air temperature on typical days or average air temperature for a long-time scale could also be used as T_R .

$$T_{N,i} = C_i \times T_R, \quad (2)$$

Then, the normalized air temperatures were used to calculate the UHI magnitudes. As shown in Table 2, the 50 PMSs were located in 11 LCZ types. The average value of UHI magnitude on the i^{th} observing site (ΔT_i) could be estimated by Equation (3).

$$\Delta T_i = T_{N,i} - T_B, \quad (3)$$

where, $T_{N,i}$ is the normalized average air temperature of the i^{th} PMS; T_B is the background air temperature, which was usually set to be the air temperature measure in rural or above water surface. For PMSs, that located in the same LCZ type, they were adopted to represent the average UHI magnitude of the LCZ type, which was denoted as $\Delta T_{LCZ,i}$. In the current work, an additional measurement on the air temperature above the water surface (LCZ G) was carried out, getting the background air temperature $T_B = 32.0$ °C.

3. Results and Discussions

3.1. Initial Measured and Normalized Air Temperatures

Table 2 provided the initially measured and normalized air temperatures on the measurement sites. Results showed that the relative values of normalized air temperature measured on different sites were not coincident with those initially measured. For example, the initially measured air temperature on the measurement site 49 (which was LCZ B), 35.1 °C, was higher than that on site 36 (which was LCZ 2), 33.1 °C; while the normalized temperature on site 36 (30.6 °C) was higher than that on site 49 (28.8 °C), as shown in Figure 4. The air temperature on site 49 was measured on 19–21 July 2014, with background air temperature 42–28 °C; while that on site 36 was measured on 13–14 July 2014, with background air temperature 38–23 °C.

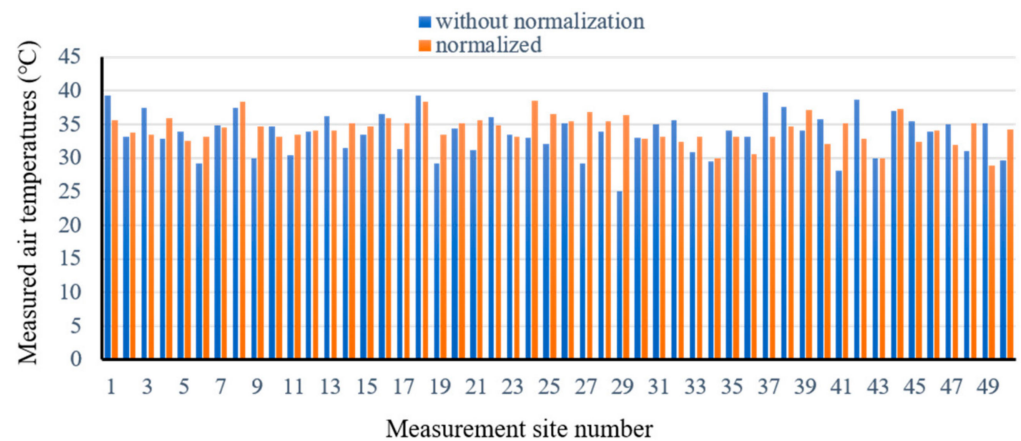


Figure 4. Comparison of air temperatures with and without normalization.

3.2. UHI Characteristics between LCZs Based on the Normalized Data

Equation (3) was used to calculate the average value of UHI magnitude on the observed sites. Figure 5 compared the daytime UHI intensity between different LCZ types, in which the measured air temperatures on each PMS site were normalized on three typical days, 5–7 June. The three typical days were clear and calm days, as Stewart and Oke [6] did in their work. It clearly illustrated the difference of UHI magnitudes between LCZ types. A daytime “cold island” formed in LCZ B, as it is covered with relatively dense tree plantings. It is well known that the shading effects of tree plantings could be mitigated by the increase of air temperature, and also, the transpiration and evaporation of tree plantings could be taking away a lot of latent heat in the vegetation-covered areas [42]. The “cold island” characteristics were also reported by Beck et al. [20] and Stewart and Oke [6] with clear and calm nighttime UHI measurement data.

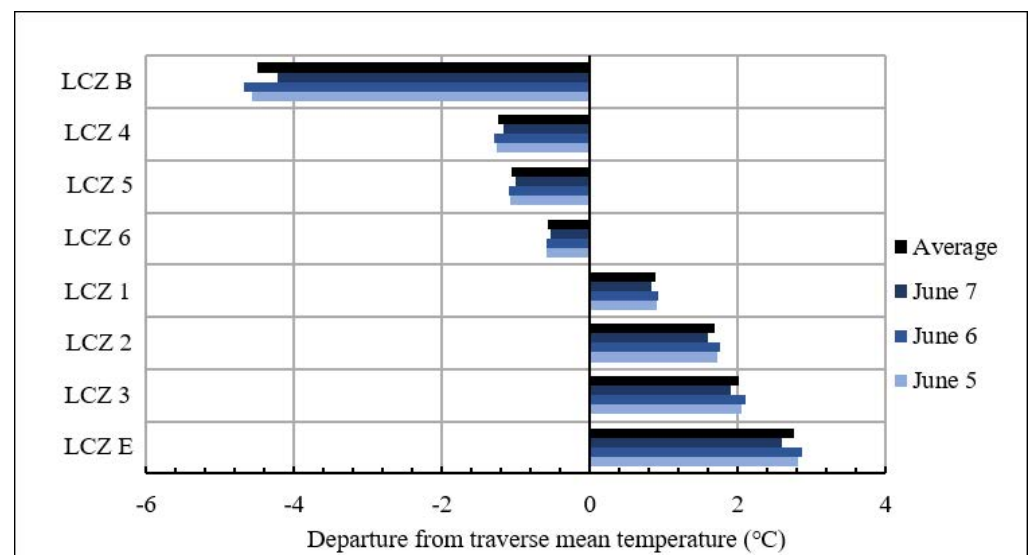


Figure 5. Comparison of urban heat island (UHI) magnitude between different local climate zone (LCZ) types.

For LCZ 4, LCZ 5 and LCZ 6, all of them are covered by open building and relatively more tree planting, thus air temperatures are lower than the traverse mean air temperature (with $\Delta T_{LCZ,i} < 0$), as shown in Figure 5. In areas of LCZ 1, LCZ 2 and LCZ 3, with compact building and less tree planting, the air temperatures are higher than the traverse mean air temperature (with $\Delta T_{LCZ,i} > 0$). This revealed the remarkable influence of land coverage and surface structure properties on local thermal environment in urban areas of Xi'an, under hot summer climate. Similar discoveries were reported by Stewart and Oke [6] and Unger et al. [28] as well.

Beside the effects of tree plantings, the building height and surface fraction are important factors influencing the UHI magnitude in built-up areas as well. The main difference between LCZ 1 and LCZ 4 is the building surface fraction, while LCZ 1 had higher building surface fraction than LCZ 4. The same situations exist between LCZ 2 and LCZ 5, and LCZ 3 and LCZ 6. As shown in Figure 5, $\Delta T_{LCZ,1} > \Delta T_{LCZ,4}$, $\Delta T_{LCZ,2} > \Delta T_{LCZ,5}$ and $\Delta T_{LCZ,3} > \Delta T_{LCZ,6}$, indicating the air temperatures in high-surface-fraction building covered areas would be higher than that in low-surface-fraction building covered areas.

On the other hand, in areas of LCZ 1, LCZ 2 and LCZ 3, which are all covered with high-surface-fraction building, but the building heights are high-rise, mid-rise and low-rise, respectively, tall buildings could provide more shielding on the pedestrian level. The UHI magnitudes were $\Delta T_{LCZ,1} < \Delta T_{LCZ,2} < \Delta T_{LCZ,3}$. The same situation existed between LCZ 4, LCZ 5 and LCZ 6, where $\Delta T_{LCZ,4} < \Delta T_{LCZ,5} < \Delta T_{LCZ,6}$. For LCZ E, which was paved with almost no trees, the UHI magnitude was very high, as there was no shielding effects. It seems that the shielding effects from tree plantings and buildings are main factors influencing the PLAT in urban areas under hot summer climate.

3.3. Statistical Analysis within Each LCZ Type

The UHI magnitude in blocks of the same LCZ type could be calculated by statistical analysis on the measured data with PMSs. With the measured data in Xi'an, the magnitudes of daytime UHI ($\Delta T_{LCZ,i}$) and the standard deviation were calculated, as shown in Table 3. The measured $\Delta T_{LCZ,i}$ revealed that higher building height with more shielding would result in lower $\Delta T_{LCZ,i}$, while higher building surface fraction would result in higher $\Delta T_{LCZ,i}$.

Table 3. UHI magnitude and standard deviation of statistical analysis in LCZ types.

LCZ Type	UHI Magnitude/°C	Standard Deviation/°C
LCZ 1	2.3	0.5
LCZ 2	2.5	0.6
LCZ 3	2.6	0.8
LCZ 4	1.3	0.5
LCZ 5I	1.7	0.6
LCZ 5II	1.8	0.8
LCZ 6	2.0	0.8
LCZ 8	3.6	0.6
LCZ B	0.7	1.2
LCZ D	1.4	1.0
LCZ E	3.5	0.6

Daytime UHI magnitudes of different LCZ types vary as results of surface structure and building coverage properties. UHI magnitudes of LCZ 8 and LCZ E are higher as there are less shielding and more paved land, while that of LCZ B, LCZ 4 and LCZ D are lower as there are more plantings. The maximum UHI magnitude is 6.5 °C, which is measured on the 25th site, covered by large low-rise buildings (LCZ 8). The average UHI magnitude for all the 11 LCZ types is 2.1 °C, which is lower than the winter UHI magnitude in Xi'an that was reported by Liu et al. [38]. Jiang et al. [43] reviewed the maximum UHI magnitudes investigated in 50 cities, and showed they are 0.9–6.1 °C, with an average value of 3.1 °C. The maximum UHI magnitude in the current work is a little higher than the reported data.

It should be noted that, in the current work, the UHI magnitudes are calculated against the measured air temperature above water surface. It should also be noted that, in the current work, only the measured data on sunny days are used to calculate the maximum daytime UHI magnitude, which would promote the UHI intensity.

The standard deviation values in Table 3 can reveal UHI magnitude difference within each LCZ type. Most of the standard deviations are less than 1.0 °C, except for that of LCZ B and LCZ D. The larger standard deviations may result from the less observing sites, as shown in Table 2. In general, the standard deviation values are lower than the reported values [44,45]. Lau et al. [44] proposed a larger daytime UHI magnitude difference of 5.4 °C in Hong Kong, while Skarbit et al. [45] illustrated it was only 1.0 °C in Szeged, Hungary. At present, investigation on reasons influencing the UHI magnitude within a LCZ type is still rare.

3.4. An Empirical Model for UHI Mapping

The UHI magnitudes of different LCZ types are related to the surface structure and land coverage types. Thus the UHI map provided by spatial interpolation on in situ measured results would be unreasonable, as the land cover characteristics of urban canopy layer do not always vary continuously in the horizontal space. The concept of LCZ provides a new feasible way for preparing an UHI map, by assigning UHI magnitude to blocks of the same LCZ type. In the current work, an empirical model for UHI mapping was proposed. In the currently proposed empirical model, the urban areas should be classified into different LCZ types firstly, in order to get the LCZ map. Then the average UHI magnitudes for each LCZ type would be calculated based on the measured data. By assigning the average UHI magnitudes of different LCZ types to blocks according to the LCZ map, an UHI map would be predicted. The statistical analysis results in Table 3 were used to map the daytime UHI distribution in Xi'an, based on the LCZ classification results as shown in Figure 2. Figure 6 illustrated the predicted daytime UHI map in Xi'an with the empirical model.

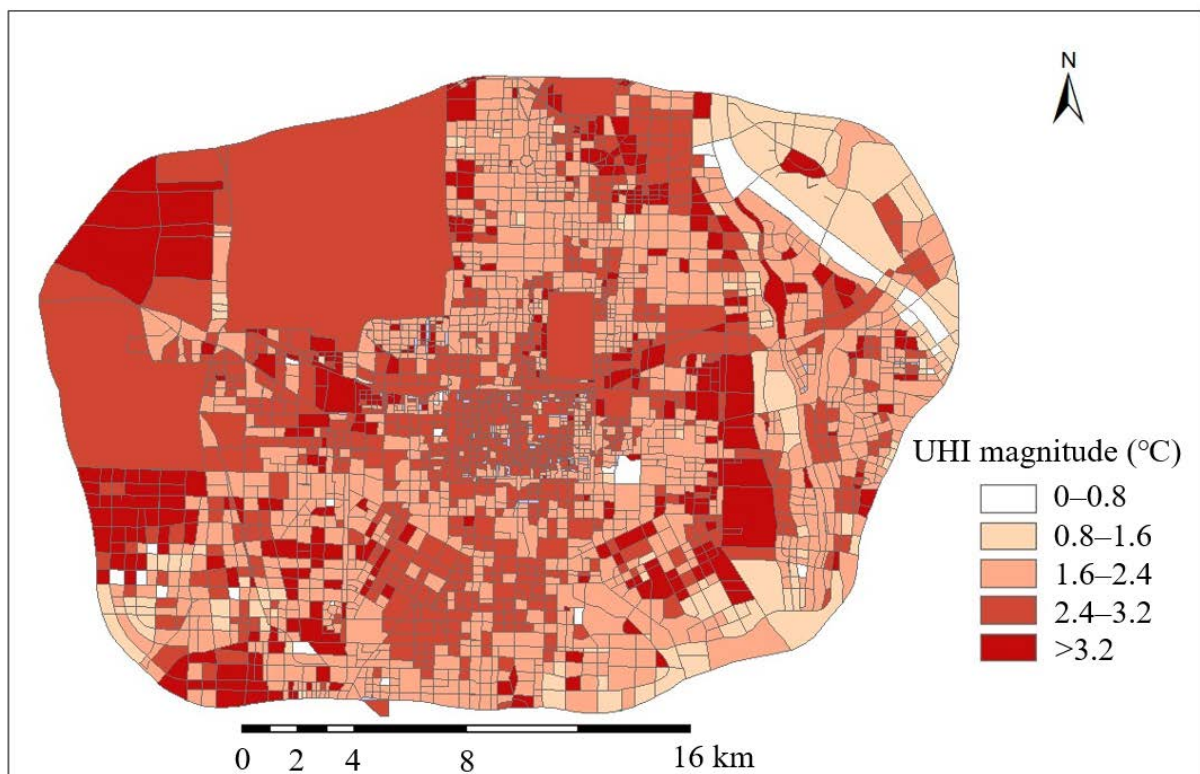


Figure 6. Map of daytime UHI in summer of Xi'an, China.

As shown in Figure 6, the daytime UHI magnitude in the urban canopy layer of Xi'an was generally high. As illustrated in Figure 2, LCZ 2 dominated in the center areas of the city, which is covered by compact mid-rise buildings, with much less greening coverage. Thus, the UHI magnitude in the center areas of the city was high, with the average value between 2.4–3.2 °C. In the northwest part of the city and in the areas outside the Eastern Second Ring Road, the dominant LCZ type was LCZ 3, which is covered by compact low-rise buildings, with much less greening coverage, leading to the high observed PLAT values in these areas. On the contrary, in the southwest and the northeast of urban, there were new development zones with fine greening coverage and a few open high-rise residential or commercial buildings, thus, the observed PLAT in these areas were generally low. Overall, the predicted daytime UHI distribution map could reasonably reflect the main spatial characteristics of UHI in Xi'an.

Xu et al. [29] also predicted the air temperature distribution in Xi'an by spatial interpolation, based on the same data set measured in the CS-UC project in Xi'an. Xu et al.'s results demonstrated that air temperatures in the central and the northwest parts of the city were higher [29], which was similar with the current work. However, the distribution of air temperature outside the Second Ring Road showed clear difference from the current work [29], especially in the southern part of the urban area. Any less of observing sites would have serious influence on the accuracy of the spatial interpolation method.

The theoretical analysis and results comparison show that the currently proposed empirical model could predict an accurate UHI map. However, a quantitative validation is still very difficult. Although there were 50 sites observed, it is still impossible to cover all the LCZs with the geographical position considered. Larger daytime UHI magnitude difference have been reported in Hong Kong, a coastal city [44], which would be also related to the topography; and also, in constructing the empirical UHI model by statistical analysis, effects from the neighborhood blocks and the anthropogenic heat emission were ignored. Thus, to get a more accurate UHI map, modifications on the empirical UHI model will consider the effects of neighborhood blocks, anthropogenic heat emission, topography and the geographical position. The current work proposed an attempt to predict the UHI map based on LCZ classification results. Only a case study in Xi'an was delivered. Modifications on the empirical model should be supported by more observation data and application practices.

4. Conclusions

The method of pedestrian-level air temperature measurement with portable micro-environment stations is practical in multi-site observations. Comparisons between the UHI magnitudes within different LCZ types revealed the significant influence of land coverage and surface structure properties on the local thermal environment. In the daytime, "cold island" would be formed within LCZ B, as the dense tree planting coverage. In areas with similar building height and different building surface fraction, results show that, $\Delta T_{LCZ,1} > \Delta T_{LCZ,4}$, $\Delta T_{LCZ,2} > \Delta T_{LCZ,5}$ and $\Delta T_{LCZ,3} > \Delta T_{LCZ,6}$. It indicates that the PLAT in high-surface-fraction building covered areas is higher than that in low-surface-fraction building covered areas. In areas covered by compact buildings, the UHI intensities vary as $\Delta T_{LCZ,1} < \Delta T_{LCZ,2} < \Delta T_{LCZ,3}$ and $\Delta T_{LCZ,4} < \Delta T_{LCZ,5} < \Delta T_{LCZ,6}$. It revealed that building height variation influences the daytime UHI magnitude as well. For LCZ E, which is paved with almost no trees, the daytime UHI magnitude is very high, as there is no shielding.

An empirical UHI mapping model was proposed by assigning average UHI magnitudes to blocks of different LCZ types, and was used to investigate the spatial characteristics of UHI in the urban areas of Xi'an, China. The UHI magnitude in areas dominated with LCZ 2 and LCZ 3 was higher, while it was lower in the new development zones with fine greening coverage and a few open high-rise residential or commercial buildings. In general, the maximum UHI magnitude in the current work is a little higher than the reported results, while the standard deviation are of low values. The predicted UHI map with the empirical model could reasonably reflect the main spatial characteristics of UHI in Xi'an City.

In perspective, the empirical UHI mapping model based on LCZ map and the in situ measured data could be a feasible and convenient way to predict the UHI map in urban areas, which would be helpful for sustainable urban planning and building design for the purpose of mitigating the UHI problems in future urban development. The normalization method should be an important component of the empirical UHI mapping model, as the observations are generally non-simultaneous. To improve the accuracy of the empirical UHI mapping model, impact factors such as the effects of neighborhood blocks, anthropogenic heat emission, topography and the geographical position could be considered.

Author Contributions: Conceptualization, Y.Z., D.Z. and Z.G.; methodology, J.Z. and Y.Z.; investigation, J.Z. and X.Z.; writing—original draft preparation, J.Z. and Y.Z.; writing—review and editing, Z.G. All authors have read and agreed to the published version of the manuscript.

Funding: This research was funded by the National Natural Science Foundation of China (grant numbers 41977182, 41861144021), the Open Foundation of the State Key Laboratory of Loess and Quaternary Geology (grant number SKLLQG1844), the National Science and Technology Foundation Project (grant number 2013FY112500), the Basic Research Plan of Natural Science of Shaanxi Province (grant number 2019JM-387), and the Shaanxi Provincial Key Research and Development Plan (grant number 2020ZDLSF06-02).

Acknowledgments: The authors would like to thank the graduated students, Q.R. Wang, S. He and L.Z. Jing, who have participated in the observations.

Conflicts of Interest: The authors declare no conflict of interest.

References

- National Bureau of Statistics of People's Republic of China. *Statistical Bulletin of the People's Republic of China on National Economic and Social Development*; National Bureau of Statistics of China: Beijing, China, 2017.
- Wang, G.; Tian, G.; Jombach, S.; Li, H. Mapping and Analyzing the Park Cooling Effect on Urban Heat Island in an Expanding City: A Case Study in Zhengzhou City, China. *Land* **2020**, *9*, 57. [\[CrossRef\]](#)
- Kesikoglu, M.H.; Atasever, U.H.; Ozkan, C.; Besdok, E. The usage of rusboost boosting method for classification of impervious surfaces. *ISPRS Int. J. Geo. Inf.* **2016**, *981–985*. [\[CrossRef\]](#)
- Zhang, Y.; Gu, Z. Air quality by urban design. *Nat. Geosci.* **2013**, *6*, 506. [\[CrossRef\]](#)
- Klysiak, K.; Fortuniak, K. Temporal and spatial characteristics of the urban heat island of Lodz, Poland. *Atmos. Environ.* **1999**, *33*, 3885–3895. [\[CrossRef\]](#)
- Stewart, I.D.; Oke, T.R. Local Climate Zones for Urban Temperature Studies. *Bull. Am. Meteorol. Soc.* **2012**, *93*, 1879–1900. [\[CrossRef\]](#)
- Cai, M.; Ren, C.; Xu, Y.; Lau, K.K.-L.; Wang, R. Investigating the relationship between local climate zone and land surface temperature using an improved WUDAPT methodology—A case study of Yangtze River Delta, China. *Urban Clim.* **2018**, *24*, 485–502. [\[CrossRef\]](#)
- Kotharkar, R.; Bagade, A. Local climate zone classification for Indian cities: A case study of Nagpur. *Urban Clim.* **2018**, *24*, 369–392. [\[CrossRef\]](#)
- Ramakreshnan, L.; Aghamohammadi, N.; Fong, C.S.; GhaffarianHoseini, A.; GhaffarianHoseini, A.; Wong, L.P.; Hassan, N.; Sulaiman, N.M. A critical review of Urban Heat Island phenomenon in the context of Greater Kuala Lumpur, Malaysia. *Sustain. Cities Soc.* **2018**, *39*, 99–113. [\[CrossRef\]](#)
- Yang, X.; Yao, L.; Jin, T.; Peng, L.L.; Jiang, Z.; Hu, Z.; Ye, Y. Assessing the thermal behavior of different local climate zones in the Nanjing metropolis, China. *Build. Environ.* **2018**, *137*, 171–184. [\[CrossRef\]](#)
- Du, P.; Chen, J.; Bai, X.; Han, W. Understanding the seasonal variations of land surface temperature in Nanjing urban area based on local climate zone. *Urban Clim.* **2020**, *33*, 100657. [\[CrossRef\]](#)
- Bechtel, B.; Alexander, P.J.; Böhner, J.; Ching, J.; Conrad, O.; Feddema, J.; Mills, G.; See, L.; Stewart, I. Mapping Local Climate Zones for a Worldwide Database of the Form and Function of Cities. *ISPRS Int. J. Geo. Inf.* **2015**, *4*, 199–219. [\[CrossRef\]](#)
- He, S.; Zhang, Y.; Gu, Z.; Su, J. Local climate zone classification with different source data in Xi'an, China. *Indoor Built Environ.* **2018**, *28*, 1190–1199. [\[CrossRef\]](#)
- Xu, Y.; Ren, C.; Cai, M.; Edward, N.Y.Y.; Wu, T. Classification of Local Climate Zones Using ASTER and Landsat Data for High-Density Cities. *J. Sel. Top. Appl. Earth Obs. Remote. Sens.* **2017**, *10*, 3397–3405. [\[CrossRef\]](#)
- Bechtel, B.; Alexander, P.J.; Beck, C.; Böhner, J.; Brousse, O.; Ching, J.; Demuzere, M.; Fonte, C.C.; Gál, T.; Hidalgo, J.; et al. Generating WUDAPT Level 0 data—Current status of production and evaluation. *Urban Clim.* **2019**, *27*, 24–45. [\[CrossRef\]](#)

16. Yang, J.; Jin, S.; Xiao, X.; Jin, C.; Xia, J.; Xia, J.; Li, X.; Wang, S. Local climate zone ventilation and urban land surface temperatures: Towards a performance-based and wind-sensitive planning proposal in megacities. *Sustain. Cities Soc.* **2019**, *47*, 101487. [[CrossRef](#)]
17. Zhao, C. Linking the Local Climate Zones and Land Surface Temperature to Investigate the Surface Urban Heat Island, A Case Study of San Antonio, Texas, U.S. *ISPRS Ann. Photogramm. Remote Sens. Spat. Inf. Sci.* **2018**, *4*, 277–283. [[CrossRef](#)]
18. Oke, T.R.; Mills, G.; Christen, A.; Voogt, J.A. *Urban Climate*, 1st ed.; Cambridge University Press: Cambridge, UK, 2017.
19. Stewart, I.D.; Oke, T.R.; Krayenhoff, E.S. Evaluation of the 'local climate zone' scheme using temperature observations and model simulations. *Int. J. Clim.* **2014**, *34*, 1062–1080. [[CrossRef](#)]
20. Beck, C.; Straub, A.; Breitner, S.; Cyrus, J.; Philipp, A.; Rathmann, J.; Schneider, A.; Wolf, K.; Jacobeit, J. Air temperature characteristics of local climate zones in the Augsburg urban area (Bavaria, southern Germany) under varying synoptic conditions. *Urban Clim.* **2018**, *25*, 152–166. [[CrossRef](#)]
21. Caluwaerts, S.; Hamdi, R.; Top, S.; Lauwaet, D.; Berckmans, J.; Degrauwe, D.; Dejonghe, H.; De Ridder, K.; De Troch, R.; Duchêne, F.; et al. The urban climate of Ghent, Belgium: A case study combining a high-accuracy monitoring network with numerical simulations. *Urban Clim.* **2020**, *31*, 100565. [[CrossRef](#)]
22. Liu, L.; Lin, Y.; Liu, J.; Wang, L.; Wang, D.; Shui, T.; Chen, X.; Wu, Q. Analysis of local-scale urban heat island characteristics using an integrated method of mobile measurement and GIS-based spatial interpolation. *Build. Environ.* **2017**, *117*, 191–207. [[CrossRef](#)]
23. Shi, Y.; Lau, K.K.L.; Ren, C.; Ng, E. Evaluating the local climate zone classification in high-density heterogeneous urban environment using mobile measurement. *Urban Clim.* **2018**, *25*, 167–186. [[CrossRef](#)]
24. Zhou, X.; Okaze, T.; Ren, C.; Cai, M.; Ishida, Y.; Watanabe, H.; Mochida, A. Evaluation of urban heat islands using local climate zones and the influence of sea-land breeze. *Sustain. Cities Soc.* **2020**, *55*, 102060. [[CrossRef](#)]
25. Saitoh, T.S.; Shimada, T.; Hoshi, H. Modeling and simulation of the Tokyo urban heat island. *Atmos. Environ.* **1996**, *30*, 3431–3442. [[CrossRef](#)]
26. Yamashita, S. Detailed structure of heat island phenomena from moving observations from electric tram-cars in Metropolitan Tokyo. *Atmos. Environ.* **1996**, *30*, 429–435. [[CrossRef](#)]
27. Liu, L.; Liu, J.; Lin, Y. Spatial-temporal Analysis of the Urban Heat Island of a Subtropical City by Using Mobile Measurement. *Procedia Eng.* **2016**, *169*, 55–63. [[CrossRef](#)]
28. Unger, J.; Sümeqhy, Z.; Zoboki, J. Temperature cross-section features in an urban area. *Atmospheric Res.* **2001**, *58*, 117–127. [[CrossRef](#)]
29. Xu, D.; Zhou, D.; Wang, Y.; Meng, X.; Chen, W.; Yang, Y. Temporal and spatial variations of urban climate and derivation of an urban climate map for Xi'an, China. *Sustain. Cities Soc.* **2020**, *52*, 101850. [[CrossRef](#)]
30. Zhang, Y.W.; He, S.; Gu, Z.L.; Wei, N.; Yu, C.W.; Li, X.; Zhang, R.; Sun, X.; Zhou, D. Measurement, normalization and mapping of urban-scale wind environment in Xi'an, China. *Indoor Built Environ.* **2019**, *28*, 1171–1180. [[CrossRef](#)]
31. Jusuf, S.K.; Wong, N.H.; Tan, C.L. Urban climatic map and STEVE tool for sustainable urban planning in Singapore. In Proceedings of the 27th International Conference on Passive and Low Energy Architecture, Louvain-la-Neuve, Belgium, 13–15 July 2011; pp. 219–225.
32. Ren, C.; Spit, T.; Lenzholzer, S.; Yim, S.H.L.; Heusinkveld, B.; Van Hove, B.; Chen, L.; Kupski, S.; Burghardt, R.; Katzschner, L. Urban Climate Map System for Dutch spatial planning. *Int. J. Appl. Earth Obs. Geoinf.* **2012**, *18*, 207–221. [[CrossRef](#)]
33. Zhang, W.; Zhang, C.; Wang, Z. Urban climate mapping and its application in urban planning. *J. Xi'an Univ. Archit. Technol.* **2014**, *46*, 261–265.
34. Xu, D.; Zhou, D.; Wang, Y.; Xu, W.; Yang, Y. Field measurement study on the impacts of urban spatial indicators on urban climate in a Chinese basin and static-wind city. *Build. Environ.* **2019**, *147*, 482–494. [[CrossRef](#)]
35. Conrad, O.; Bechtel, B.; Bock, M.; Dietrich, H.; Fischer, E.; Gerlitz, L.; Wehberg, J.; Wichmann, V.; Böhner, J. System for Automated Geoscientific Analyses (SAGA) v. 2.1.4. *Geosci. Model Dev.* **2015**, *8*, 1991–2007. [[CrossRef](#)]
36. Luo, X.; Yu, C.W.; Zhou, D.; Gu, Z. Challenges and adaptation to urban climate change in China: A viewpoint of urban climate and urban planning. *Indoor Built Environ.* **2019**, *28*, 1157–1161. [[CrossRef](#)]
37. Luo, X.; Gu, Z.; Tian, W.; Xia, Y.; Ma, T. Experimental study of a local ventilation strategy to protect semi-exposed relics in a site museum. *Energy Build.* **2018**, *159*, 558–571. [[CrossRef](#)]
38. Liu, J.P.; Lin, X.D.; Liu, Y.F. Survey on winter urban heat island in Xi'an. *Acta Energ. Sol. Sin.* **2007**, *28*, 912–917.
39. Sakakibara, Y.; Matsui, E. Relation between Heat Island Intensity and City Size Indices/Urban Canopy Characteristics in Settlements of Nagano Basin, Japan. *Geogr. Rev. Jpn.* **2005**, *78*, 812–824. [[CrossRef](#)]
40. Leconte, F.; Bouyer, J.; Claverie, R.; Pétrissans, M. Using Local Climate Zone scheme for UHI assessment: Evaluation of the method using mobile measurements. *Build. Environ.* **2015**, *83*, 39–49. [[CrossRef](#)]
41. Wang, Z.; Lu, J. A Mathematic Model for Calculating Urban Heat Island Intensity Using Mobile Survey Data. In Proceedings of the Lecture Notes in Electrical Engineering; Springer Science and Business Media LLC: Berlin, Germany, 2013; Volume 261, pp. 563–572.
42. Vera, S.; Pinto, C.; Tabares-Velasco, P.C.; Bustamante, W. A critical review of heat and mass transfer in vegetative roof models used in building energy and urban environment simulation tools. *Appl. Energy.* **2018**, *232*, 752–764. [[CrossRef](#)]

43. Jiang, S.; Zhan, W.; Yang, J.; Liu, Z.; Huang, F.; Lai, J.; Li, J.; Hong, F.; Huang, Y.; Chen, J.; et al. Urban heat island studies based on local climate zones: A systematic overview. *Acta Geogr. Sin.* **2020**, *75*, 1860–1878.
44. Lau, K.K.L.; Chung, S.C.; Ren, C. Outdoor thermal comfort in different urban settings of sub-tropical high-density cities: An approach of adopting local climate zone (LCZ) classification. *Build. Environ.* **2019**, *154*, 227–238. [[CrossRef](#)]
45. Skarbit, N.; Stewart, I.D.; Unger, J.; Gál, T. Employing an urban meteorological network to monitor air temperature conditions in the 'local climate zones' of Szeged, Hungary. *Int. J. Clim.* **2017**, *37*, 582–596. [[CrossRef](#)]